

## PAPER



Cite this: *J. Mater. Chem. A*, 2017, 5, 13601

## Hybrid lithium-ion capacitors with asymmetric graphene electrodes†

Yige Sun,<sup>ab</sup> Jie Tang, <sup>ab</sup> Faxiang Qin,<sup>ac</sup> Jinshi Yuan,<sup>a</sup> Kun Zhang,<sup>a</sup> Jing Li,<sup>ab</sup> Da-Ming Zhu<sup>d</sup> and Lu-Chang Qin<sup>e</sup>

The dramatically increased demand for electric devices such as electric vehicles and consumer electronics prompted us to explore new ideas in fabricating novel energy storage devices. In this work, we designed, constructed, and studied an asymmetric hybrid lithium-ion capacitor (LIC) by combining an electric double-layer capacitor cathode and a lithium-ion battery anode. Both electrodes were made of a single-wall carbon nanotube and graphene (SG) composite to reduce restacking of the graphene nanosheets, to improve the energy storage capacity, and to improve the electrical conductivity of the electrodes. One of the electrodes was pre-lithiated electrochemically. After pre-lithiation, the lithiated-SG (Li-SG) electrode showed excellent capacity in lithium intercalation and de-intercalation and was used as the anode of the LIC device. The advantage of the hybrid LIC with asymmetric graphene electrodes is that it maximizes the operable voltage between the two electrodes, thus increasing the energy density of the device. The hybrid LIC fabricated in this work exhibited an energy density of 222 W h kg<sup>-1</sup> at a power density of 410 W kg<sup>-1</sup>.

Received 5th February 2017  
Accepted 5th May 2017

DOI: 10.1039/c7ta01113j

rsc.li/materials-a

### 1. Introduction

In the past decades, there has been a dramatic increase in the demand for improved energy storage devices due to the rapid development of portable electronics and electric vehicles.<sup>1,2</sup> Among the most widely used energy storage devices, electric double-layer capacitors (EDLCs) can offer a high specific power and long cycle life, though their relatively low energy density has largely limited their applications. On the other hand, lithium-ion batteries (LIBs) can deliver a high energy density, but their applications are often limited by their low power density.<sup>1-3</sup> A recent technological innovation has been the development of lithium-ion capacitors – they combine the advantages of the high power density of EDLCs and high energy density of LIBs by using one EDLC electrode and one LIB electrode in constructing the LIC device.

For an LIC cell, faradaic processes occur on the anode (LIB electrode) and it usually has a much larger capacity than the cathode (EDLC electrode) that undergoes non-faradaic reactions. Therefore the capacitance of an LIC device is about twice that of an EDLC constructed symmetrically.<sup>4-6</sup> In addition, a carbon electrode without pre-lithiation usually has a high electrochemical potential at around 3 V with respect to a Li/Li<sup>+</sup> electrode and therefore carbon materials, such as activated carbon (AC) and graphite, are usually used as the positive electrode (cathode). However, after pre-lithiation, the electrochemical potential of the doped carbon material could drop significantly. As a result, the open circuit voltage for an LIC full-cell would increase substantially when the pre-lithiated carbon electrode is utilized as the anode in order to improve the energy storage capacity.<sup>1,7-9</sup>

Many efforts have been made in fabricating LIC devices and understanding their operating mechanisms in order to determine the direction of further improvement.<sup>3,4,7,10</sup> For example, Dahn *et al.* reported an analysis of dual-graphite cells in comparison with LIB cells.<sup>3</sup> In these dual-graphite cells, Li ions were intercalated into the graphite anode, while PF<sub>6</sub><sup>-</sup> ions were adsorbed onto the graphite cathode. Amatrice *et al.* reported a non-aqueous asymmetric electrochemical cell with AC as the cathode and nanostructured Li<sub>4</sub>Ti<sub>5</sub>O<sub>12</sub> as the anode, which provided extended cycle life and fast charge capability, as well as a 400–500% increment in energy density compared with an EDLC.<sup>4</sup> In this LIC device, the adsorption and desorption of the anions took place on the surface of the AC electrode (cathode) which underwent a non-faradaic process and displayed an

<sup>a</sup>National Institute for Materials Science, 1-2-1 Sengen, Tsukuba, Ibaraki 305-0047, Japan. E-mail: tang.jie@nims.go.jp

<sup>b</sup>Doctoral Program in Materials Science and Engineering, University of Tsukuba, 1-1-1 Tennodai, Tsukuba, Ibaraki 305-8577, Japan

<sup>c</sup>Institute for Composite Science Innovation (InCSI), School of Materials Science and Engineering, Zhejiang University, Hangzhou, Zhejiang 310058, China

<sup>d</sup>Department of Physics and Astronomy, University of Missouri-Kansas City, Kansas City, MO 64110, USA

<sup>e</sup>Department of Physics and Astronomy, University of North Carolina at Chapel Hill, Chapel Hill, NC 27599-3255, USA

† Electronic supplementary information (ESI) available. See DOI: 10.1039/c7ta01113j

electrochemical behaviour of EDLCs. The intercalation and de-intercalation of Li ions occurred on the negative  $\text{Li}_4\text{Ti}_5\text{O}_{12}$  electrode (anode) which exhibited a reversible high capacity and underwent a faradaic process during charging/discharging. This AC// $\text{Li}_4\text{Ti}_5\text{O}_{12}$  (cathode//anode) LIC offered a remarkable high energy density of  $85 \text{ W h kg}^{-1}$ .<sup>4</sup> Another alternative approach to further increasing the energy density of LICs is to use a more effective electrolyte. Béguin *et al.* developed an organic electrolyte for AC//graphite capacitors and achieved a high energy density of  $103.8 \text{ W h kg}^{-1}$ .<sup>7</sup>

To further increase the energy density of an LIC device, searching for new electrode materials with larger capacitance for both electrodes has attracted considerable amount of attention in materials research as such electrode materials will lead to an improvement of the capacitance of the whole LIC cell.<sup>11–15</sup> For the cathode (EDLC electrode), graphene and graphene-based materials have appeared to be extremely attractive over traditional AC due to their excellent properties, including large specific surface area ( $2630 \text{ m}^2 \text{ g}^{-1}$ ), high electrical conductivity, and excellent electrochemical stability.<sup>16–20</sup> On the other hand, since graphene offers a very high diffusivity for Li ions (about  $10^{-7}$  to  $10^{-6} \text{ cm}^2 \text{ s}^{-1}$ ), it has also been regarded as an anode material of great potential in LIC applications.<sup>12,21,22</sup> A number of recent studies have demonstrated the great performance of graphene electrodes in hybrid LICs.<sup>14,15</sup> In these studies, various types of graphene-based materials were studied for both cathode and anode applications. For example, an all-graphene battery, using functionalized graphene as the cathode and reduced graphene oxide as the anode, delivered an energy density of  $225 \text{ W h kg}^{-1}$  (ref. 14) and a hybrid LIC with pure graphene as the electrode material showed an energy density of  $148.3 \text{ W h kg}^{-1}$ .<sup>15</sup>

In our previous work, we developed a process to fabricate a single-wall carbon nanotube (SWCNT) and graphene (SG) composite that showed improved electric conductivity, electrolyte ion diffusion, structural stability, and high porosity.<sup>19,23</sup> One of the major advantages in using the SG composite as the electrode material is that the carbon nanotubes inserted in between the graphene nanosheets could result in a well-mixed three-dimensional carbon nanotube/graphene network which can effectively prevent or reduce the restacking of graphene without lowering its electrical conductivity. When it is used as the electrodes of a symmetric EDLC, the graphene supercapacitor showed both high energy density and high power density.<sup>19</sup> However, there has been no report on experimental investigations of the possible advantages of utilizing the carbon nanotube/graphene composite as the electrode material for LICs.

In this work, we expand the uses of the SG composite electrode and report the construction and characterization of a hybrid LIC using the SG composite for both the cathode and anode. In assembling the LIC device, the cathode was prepared using the pristine SG composite directly, while the anode was prepared with pre-lithiation of the pristine SG composite. The novelty of this work is to take full advantage of the SG electrode in both faradaic processes (anode) and non-faradaic process (cathode). As mentioned above, the SG composite electrode can

effectively prevent graphene from stacking, enhance the electrolyte ion adsorption/desorption, and provide favourable paths for Li-ion diffusion. As will be described in detail in this report, the asymmetric hybrid LIC developed in this work exhibited an energy density of  $222 \text{ W h kg}^{-1}$  and a power density of  $410 \text{ W kg}^{-1}$  with good cycling characteristics in comparison with similar devices using either SWCNTs or graphene alone as the electrode material.<sup>15,19</sup>

## 2. Experimental

### 2.1 Synthesis of the SG composite

Graphene oxide (GO) was synthesized from graphite flakes using a modified Hummers' method. The details of the method were already reported in our previous publication.<sup>19</sup> Specifically, graphite flakes (median size 7–10 micron, Alfa Aesar) and  $\text{NaNO}_3$  (Nacalai Tesque) were mixed first by stirring them in a beaker and followed by adding successively  $\text{H}_2\text{SO}_4$  (Nacalai Tesque) and  $\text{KMnO}_4$  (Chameleon Reagent) into the mixture in an ice-water bath. The mixture was then stirred at room temperature before it was dissolved in deionized water to obtain a brown coloured suspension. After adding  $\text{H}_2\text{O}_2$  (Santoku Chemical Industries) to the suspension, the colour of the suspension would turn to yellow with some effervescence during the reactions. Centrifugation was used to improve the purification of the GO platelets. In order to exfoliate the graphite oxide into graphene oxide (GO) platelets, the bright yellow suspension was centrifuged at 35 000 rpm for 30 minutes several times until the pH value reached 7. Finally, the GO platelets were dispersed in deionized water to serve as the precursor for preparing the SG composite.

The SG composite was prepared by mixing SWCNTs (Cheap Tube, Inc.) and GO first aided by sonication. Once the SWCNTs were well dispersed in the GO suspension, reduction was carried out by adding hydrazine monohydrate ( $\text{H}_2\text{NNH}_2 \cdot \text{H}_2\text{O}$ , Wako Pure Chemical Industries) into the suspension. The mixture suspension was then filtered to obtain an SG slurry. The slurry was finally washed with distilled water and vacuum-dried to obtain the SG composite in the form of dried powders.

### 2.2 Fabrication of the working electrode

In fabricating the working electrode, the SG composite powders were first dispersed in ethanol (Nacalai Tesque) and the suspension was then filtered onto a weighted porous filter membrane, followed by drying in a vacuum at  $110^\circ \text{C}$  for 12 hours to remove water and ethanol. The areal mass densities were 1 and  $7 \text{ mg cm}^{-2}$  to meet the balanced mass ratio between the cathode and anode of 6.76.

### 2.3 Pre-lithiation of the anode

An SG//Li half-cell (CR2032-type coin cell) was utilized for the pre-lithiation of the SG electrode. The half-cell includes a piece of polypropylene as the separator, a lithium foil as the source of lithium, and a counter electrode. The electrolyte was  $\text{LiPF}_6$  ( $1 \text{ mol L}^{-1}$  in EC : DMC = 1 : 1 (v/v%)). The open-circuit voltage (OCV) of the half-cell was typically about 3 V before lithiation.

Pre-lithiation was carried out by discharging to achieve lithium intercalation at a constant current density of  $50 \text{ mA g}^{-1}$  during which the OCV would drop eventually to 0.01 V. In the process of discharging, the formation of a solid electrolyte interphase (SEI) usually leads to an irreversible capacity.<sup>24,25</sup> The formation of the SEI layer would also cause a slight increase of the electrode mass at  $60\text{--}90 \mu\text{g cm}^{-2}$ .<sup>26</sup> The resultant mass change was about 0.85–8.26% of the mass of the electrode ( $1\text{--}7 \text{ mg cm}^{-2}$ ) in this study. The capacity of the anode would show a stable behaviour after the first 3 cycles were completed. At the end of the third cycle, when the potential of the SG anode reached 0.01 V, the anode was disconnected from the circuit and it is ready to be used as the anode of the LIC cell. This process of lithiation could also cause a slight increase of the mass of the electrode.

#### 2.4 Structural characterization of the materials

The crystalline phases and compositions of the material samples were all characterized by powder X-ray diffraction (XRD, Rigaku SmartLab using Cu-K $\alpha$  radiation with  $\lambda = 1.5418 \text{ \AA}$ ). The morphology and microstructure of the precursor material, graphene oxide, and SG composite were examined using scanning electron microscopy (SEM, JSM-6500), transmission electron microscopy (TEM, JEM-2100), and atomic force microscopy (AFM, JSPM-5200). X-ray photoelectron spectroscopy (XPS, PHI Quantira SXM, ULVAC-PHI) was used to analyse the chemical composition of and bonding configurations in the SG composite. Raman spectroscopy (RAMAN-11 with a 532 nm laser source, Nanophoton) was used to characterize the D-band and the G-band peaks associated with the graphitic structure in the SG composite.

#### 2.5 Electrochemical characterization

The electrochemical performance of all finished cells was tested in a glovebox filled with argon gas. All the EDLC cells were characterized in the two-electrode configuration. The applied potential window was from 0 to 2.7 V. Half-cells with lithium foil as the reference electrode, denoted as SG//Li, were used to study the electrochemical performance of the electrode material between 0.01 and 3 V. Three-electrode cells were also used for analysing the electrochemical performance of the LIC full-cells (SG//Li//Li-SG) between 0.01 and 4.1 V (mass ratio between the cathode and anode is 6.76). The same polypropylene separator and  $\text{LiPF}_6$  electrolyte were used in all cells. Cyclic voltammetry and galvanostatic charge/discharge measurements at increasing current densities were carried out using a VMP3 multi-potentiostat/galvanostat (Biologic) system at room temperature.

## 3. Results and discussion

### 3.1 Structure and morphology of the SG composite

Fig. 1 shows the structural characterization of the SG composite. All the images were taken after the material samples were dried. There is no evidence suggesting that the drying process caused aggregation in the SG composite. Fig. 1a shows a typical high-resolution electron micrograph where well-

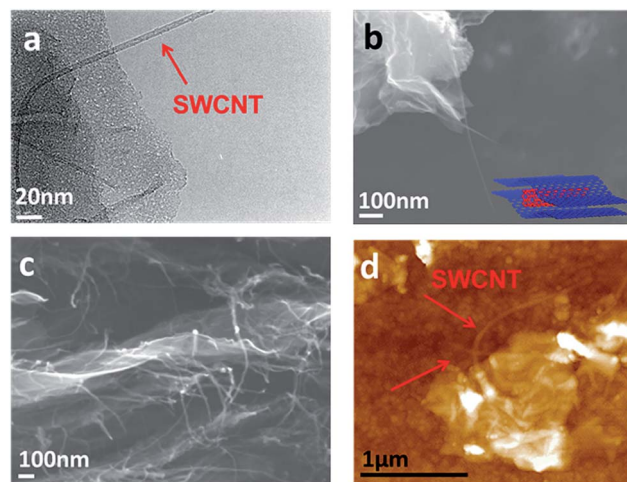


Fig. 1 Structural characterization of the single-wall carbon nanotube (SWCNT) and graphene (SG) composite. (a) Transmission electron microscopy (TEM) image revealing homogeneous distribution of SWCNTs; (b and c) scanning electron microscopy (SEM) images (inset is a schematic illustration of the configuration of graphene sheets with a carbon nanotube in between); and (d) atomic force microscopy (AFM) image of the same SG composite. Arrows indicate single-wall carbon nanotubes in the images.

dispersed SWCNTs were resolved clearly. At a finer scale, as shown in the SEM images given in Fig. 1b and c, the SWCNTs were distributed homogeneously in between the graphene nanosheets. We did not observe any other configurations, such as separation of SWCNTs and graphene or aggregation of carbon nanotubes in the electrode material that we have prepared. The three-dimensional (3D) network structure of the SG composite should reduce effectively the restacking of graphene nanosheets to result in more intra-pores and a larger specific surface area of  $950 \text{ m}^2 \text{ g}^{-1}$  to adsorb  $\text{PF}_6^-$  anions effectively.<sup>19</sup> In addition, the 3D network structure with SWCNT spacers should also produce favourable diffusive paths for intercalation/de-intercalation of Li ions and increase the structural stability of the electrode.

X-ray diffraction patterns of GO, SWCNTs, the SG composite, and chemically reduced graphene (CRG) without single-wall carbon nanotubes are shown in Fig. 2a. GO showed a much larger characteristic interlayer spacing ( $d \sim 0.73 \text{ nm}$ ). This is attributed to the existence of oxygen functional groups and water molecules sitting in between the GO sheets.<sup>27</sup> The weak and broad peak due to the SG composite indicates a structure with an interlayer spacing of  $d \sim 0.450 \text{ nm}$ , which is much larger than that observed in CRG ( $d \sim 0.342 \text{ nm}$ ). This dramatic increase in the interlayer spacing in the SG composite is attributed to the presence and function of SWCNTs that served as spacers and presence of  $\pi$ -electron macromolecules.<sup>28</sup> When compared to the corresponding Bragg peak of CRG, the broader peak of the SG composite also indicates more disorders in the distribution of the graphene layers with SWCNTs inserted in between them. Fig. 2b shows the Raman D-band and G-band of the SG composite and pristine CRG. The G-peak corresponds to the high-frequency  $E_{2g}$  phonons at the centre of the Brillouin

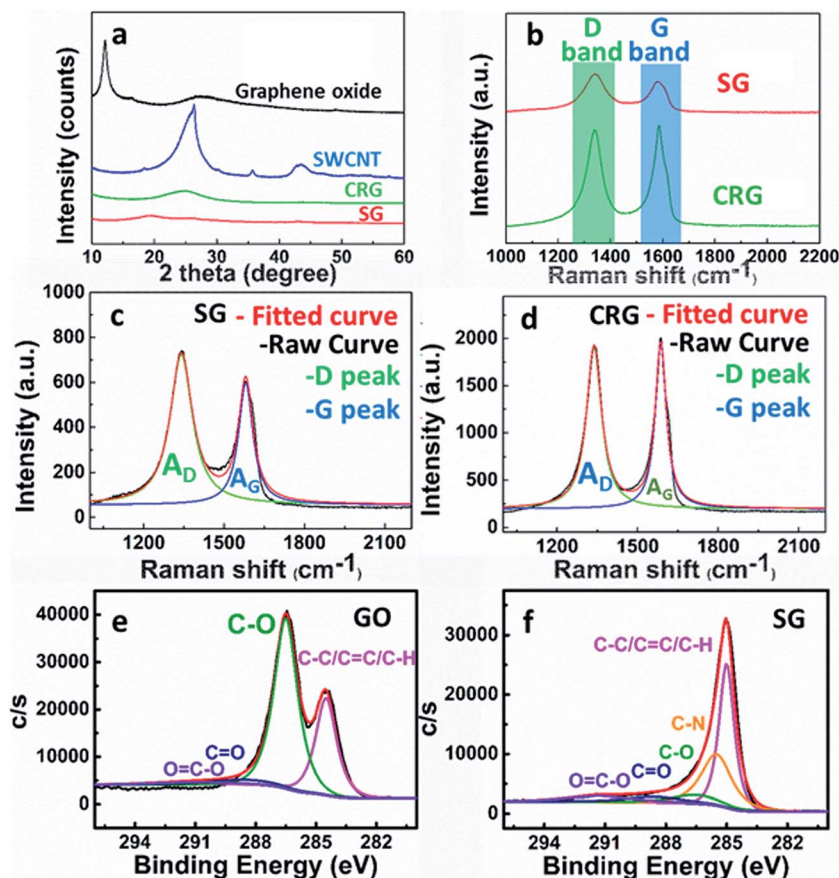


Fig. 2 (a) X-ray diffraction patterns of graphene oxide (GO), reduced graphene oxide (CRG), single-wall carbon nanotubes (SWCNTs), and the SWCNT/SG composite; (b) Raman spectra of CRG and SG samples showing the D-band and G-band; (c and d) measurement of the integrated area under the Raman peaks due to the D-band ( $A_D$ ) and the G-band ( $A_G$ ) by curve fitting of the original Raman data shown in (b).  $A_D/A_G$  in SG is substantially greater than that in CRG; (e) analysis of  $C_{1s}$  X-ray photoelectron spectra of GO and (f) SG. Identified C-containing functional groups in the samples are also given in the respective figure.

zone and it is related to the relative motion of  $sp^2$  bonded graphitic carbon atoms.<sup>29</sup> The D-peak is due to the breathing modes of the typical six-atom rings, indicating disorders in the graphitic structure. The ratio of the integrated area under the D and G peaks,  $A_D/A_G$ , quantifies disorder in graphene.<sup>30</sup> As shown in Fig. 2c and d, which include the fitted curves of the D- and G-peaks, the  $A_D/A_G$  ratio for the SG composite is 1.85, which is 40% greater than that for CRG (1.31). This should also be due to integration of SWCNTs into the 3D network structure and the increased bridge-defects between the SWCNTs and graphene nanosheets.<sup>31</sup> In addition, as can be observed in the fitted curves given in Fig. 2c, the full-width at half maximum (FWHM) of the G peak for the SG composite was  $64.85\text{ cm}^{-1}$ , which was about 30% larger than the FWHM of the G-peak for CRG given in Fig. 2d ( $50.53\text{ cm}^{-1}$ ). This result indicates a greater degree of disorder in the SG composite than that in CRG,<sup>32</sup> in agreement with the XRD result discussed above (Fig. 2a).

The XPS spectra of GO and the SG composite are shown in Fig. 2e and f, respectively. The GO spectrum shows a pronounced peak at 286.5 eV, attributed to the C–O bond. The  $C_{1s}$  spectrum of the SG composite can be divided into several sub-peaks: a significantly strong peak due to graphitic carbon

(C–C, C=C, and C–H bonds: 284.5 eV), a peak due to the C–N bonds (285.5 eV) as a result of reactions between hydrazine monohydrate and carbon, and weak peaks due to carbon combined with O (C–O bonds (286.5 eV), C=O bonds (288.6 eV) and carboxyl groups O=C–O (291.3 eV)). The decreased intensity due to the C–O bond compared with that from GO indicates the removal of oxygen functional groups in GO. The C/O ratio of the starting GO precursor was only 1.72, while the C/O ratio of the finished SG composite was increased to 10.69, indicating that highly reductive reactions had taken place indeed during the preparation of the SG composite.

### 3.2 Electrochemical characterization of the SG electrode in the EDLC

As a LIC is a hybrid system, each electrode has different functions and has its own impacts on the overall performance of the LIC device. Therefore, we investigated the electrochemical behaviour of each electrode separately in our study of the LIC cell.

A non-faradaic process occurs on the cathode of the LIC, which works by a mechanism similar to that of an EDLC. In order to evaluate the electrochemical behaviour of the SG

composite as a cathode, a symmetric capacitor cell SG//SG (Fig. 3a) and a half-cell SG//Li (Fig. S2†) were assembled. The cyclic voltammograms (CV) of the SG//SG capacitor in the potential window of 0 and 2.7 V are shown in Fig. 3b. The CV loops displayed nearly rectangular shapes over scanning rates from 10 to 200 mV s<sup>-1</sup>, indicating a characteristic capacitive behaviour. The galvanostatic charge–discharge curves shown in Fig. 3c indicate an excellent rate performance (Fig. 3d). The gravimetric specific capacitance  $C_s$  (F g<sup>-1</sup>) of the electrode was calculated using the equation<sup>32–35</sup>

$$C_s = \frac{\Delta Q}{\Delta V \times m} = 4 \times \frac{I}{m} \times \frac{dt}{dV}, \quad (1)$$

where  $I$  is the loading current (A),  $m$  the total mass of both electrodes (g), and  $dt/dV$  (s V<sup>-1</sup>) is derived from the plot of the potential ( $V$ , excluding the  $IR$  drop) vs. time (second) of the galvanostatic discharge curve given in Fig. 3c. As shown in Fig. 3c, with the time of discharge of 1830 seconds and the potential window of 2.7 V, the specific capacitance of the SG electrode was 145 F g<sup>-1</sup> (capacity: 74 mA h g<sup>-1</sup>) at the current density of 0.05 (34) A g<sup>-1</sup>. This result is in excellent agreement with the half cell: SG//Li operated from 2 V to 4 V vs. Li/Li<sup>+</sup> (137 F g<sup>-1</sup> in Fig. S2b†), indicating good reproducibility of the experiment. It was slowly reduced to 101 F g<sup>-1</sup> when the current density was increased to 1.0 A g<sup>-1</sup>. This specific capacitance is much greater than that of the AC electrode in the symmetric capacitor device AC//AC that we also measured for comparison (Fig. S1†). The specific capacitance of the AC electrode was 60 F g<sup>-1</sup>, and it quickly dropped to 31 F g<sup>-1</sup>, retaining only 53% of its initial value when the current density decreased from 0.05 to 1.0 A g<sup>-1</sup>. This retention rate is much smaller than that of the SG composite (70%).

The outstanding capacity of the SG composite in the EDLC is attributed to the unique three-dimensional network structure of the composite and the extraordinary properties of the constituents: one-dimensional SWCNTs and two-dimensional graphene nanosheets. The combination of these two constituents offers a synergy of properties that out-performs each one working alone. In brief, the major advantages of the SG composite are as follows: (1) the SG composite has more functional surface area than AC, since many of the micropores in AC cannot be accessed by the electrolyte ions; (2) the use of SWCNTs as spacers prevents graphene from re-stacking in the composite; and (3) the use of SWCNTs also improves the

electrical and thermal conductivity of the composite. As discussed by Yuan *et al.*, the electrical conductivity of a SWCNT is very high in its axial direction, which should make SWCNTs excellent conductive binders in the SG composite.<sup>36–40</sup>

### 3.3 Electrochemical characterization of pre-lithiated SG (Li-SG) as an anode

In order to analyse the electrochemical performance of Li-SG as an anode in LICs, a Li-SG//Li half-cell, illustrated schematically in Fig. 4a, was assembled and operated in the potential range from 0.01 to 3.0 V. After pre-lithiation, the colour of the SG anode changed from black to golden, similar to that reported for graphite, indicating a high degree of lithiation.<sup>41</sup>

Fig. 4b and c show the cyclic voltammograms and galvanostatic charge–discharge curves of the Li-SG//Li half-cell. The CV of Li-SG (Fig. 4a) exhibited typical features of carbon electrodes. There is a broad peak at 0.7 V appearing in the first cycle, indicating the formation of a solid electrolyte interphase (SEI) film. This SEI film usually obstructs the direct contact between the electrolyte and the active electrode surface, causing decrease in the degree of Li intercalation and de-intercalation. As shown in Fig. 4c, the specific capacity for the first discharge was 1520 mA h g<sup>-1</sup>, while the specific capacity for the first charge was only 562 mA h g<sup>-1</sup> (37% of the first discharge capacity). The charge and discharge capacity became stable at about 500 mA h g<sup>-1</sup> in the following cycles and this value was taken as the maximum capacity of lithium intercalation and de-intercalation. It is much larger than that of the pre-lithiated graphite electrode (250 mA h g<sup>-1</sup> in Fig. S3†) that was treated by the same process. The rate performance of the Li-SG electrode is shown in Fig. 4d. The charge capacity of the Li-SG electrode was 503, 479, 391, 339, and 256 mA h g<sup>-1</sup> at the current densities of 50 mA g<sup>-1</sup>, 100 mA g<sup>-1</sup>, 200 mA g<sup>-1</sup>, 500 mA g<sup>-1</sup> and 1 A g<sup>-1</sup>, respectively. When the current density was decreased back to 50 mA g<sup>-1</sup>, the charge capacity would raise back to 511 mA h g<sup>-1</sup>. The Li-SG electrode also exhibited excellent cycling performance as shown in Fig. 4e. After 50 cycles, the charge capacity was still as high as 495 mA h g<sup>-1</sup>. Moreover, the coulombic efficiency was 99% and was stable. The capacity shows a slight increase during the cycling. The slight increase is attributed to improved ion diffusion kinetics and to the activation of the electrode during aging.<sup>42,43</sup>

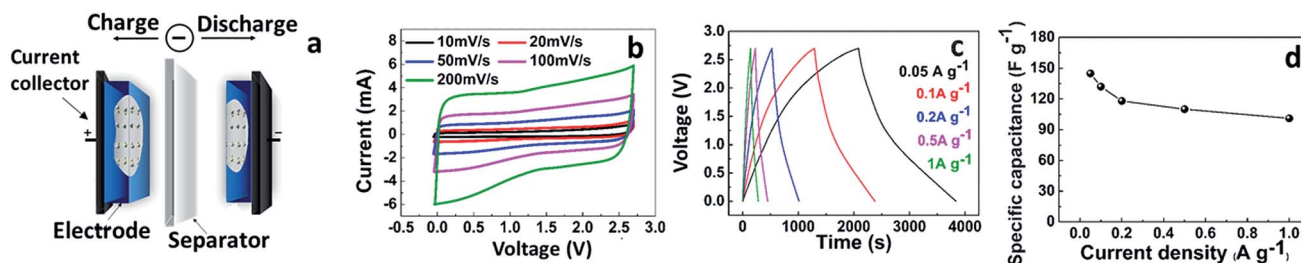


Fig. 3 (a) Schematic illustration of the SG//SG capacitor; (b) cyclic voltammograms at different scan rates from 10 to 200 mV s<sup>-1</sup>; (c) galvanostatic charge–discharge curves at various current densities, and (d) rate performance at various current densities shown in (c).

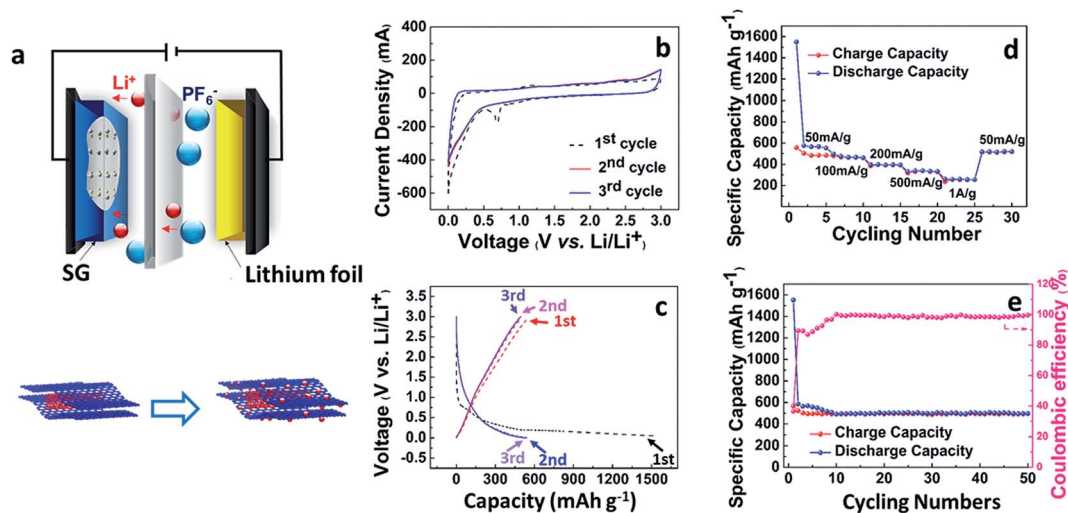


Fig. 4 (a) Schematic of the SG//Li cell structure; (b) cyclic voltammograms for the first three cycles with a scan rate of potential at  $0.1 \text{ mV s}^{-1}$ ; (c) galvanostatic charge–discharge curves at a current density of  $50 \text{ mA g}^{-1}$ ; (d) rate performance; and (e) cycling performance of the Li-SG anode.

It should be noted that the Li-SG composite delivered a specific capacity greater than the theoretical capacity of  $372 \text{ mA h g}^{-1}$  for the graphite electrode. This outstanding performance is because the three-dimensional network structure of the Li-SG composite enabled the following: (1) larger interlayer spacing ( $0.45 \text{ nm}$  as shown in Fig. 2a) than that of graphite ( $0.335 \text{ nm}$ ), which should increase the stability of the electrode during cycling (Fig. 4e) and make possible the intercalation of both Li-ions and  $\text{Li}_2$  molecules, and maybe even accommodate multiple layers of lithium ions;<sup>44,45</sup> (2) enhanced accessibility for lithium in the electrode structure in which the lithium ions could be adsorbed on both sides of the graphene nano-sheets;<sup>46,47</sup> and (3) more structural defects compared with graphite since the Li-SG composite has more disorders. These defects could react with lithium ions more effectively and further increase the capacity.<sup>44</sup> Therefore, the Li-SG composite is well positioned to replace graphite as the anode of the LIC to improve lithium intercalation and de-intercalation.

### 3.4 Electrochemical performance of dual-graphene LIC:SG//Li-SG

As described above, the specific capacity of the SG cathode was  $74 \text{ mA h g}^{-1}$  and the specific capacity of the Li-SG anode was  $500 \text{ mA h g}^{-1}$ . Therefore, in order to maintain the charge balance of the whole system,<sup>48,49</sup> the balanced mass ratio between the cathode and anode needs to be 6.76. The electrochemical performance of the SG//Li-SG LIC full-cell, schematically illustrated in Fig. 5a, is shown in Fig. 5d–f. The CV loops of the SG//Li-SG LIC (operated between  $0.01$  and  $4 \text{ V}$ ) are shown in Fig. 5b. The CV curves were stable even at the large scan rate of  $200 \text{ mV s}^{-1}$ . It should be noted that these CV loops did not display the characteristic rectangular shapes as did those in the EDLC. Fig. 5c compares the CV curves of the SG cathode ( $2$ – $4 \text{ V}$ ), the Li-SG anode ( $0.01$ – $3 \text{ V}$ ) and the SG//Li-SG LIC full-cell ( $0$ – $4 \text{ V}$ ) at the potential scan rate of  $10 \text{ mV s}^{-1}$ .

The CV loop of the SG cathode displayed an EDLC behaviour as described in Fig. 3b. On the other hand, as expected, the CV loop of the Li-SG anode showed peaks characteristic of battery behaviour due to lithium intercalation and de-intercalation. Comparing with that obtained from the SG cathode and the Li-SG anode separately, the CV loop of the SG//Li-SG LIC full-cell ( $0.01$ – $4 \text{ V}$ ) occupies a much larger enclosed area, indicating that the LIC full-cell can store more energy owing to the benefits from the LIC structure with different electrodes working in tandem. The galvanostatic charge–discharge curves of the LIC cell are shown in Fig. 5d, also indicating a good rate performance (Fig. 5e). It should be noted that there is no stable potential plateau for the LIC as displayed in Fig. 5d, a characteristic distinction in the electrochemical behaviour from an LIB. The gravimetric specific capacitance of the SG//Li-SG LIC full-cell  $C_{\text{LIC}}$  ( $\text{F g}^{-1}$ ) was calculated using

$$C_{\text{LIC}} = \frac{I}{m_{\text{cathode}+\text{anode}}} \times \frac{dt}{dV}. \quad (2)$$

At the current density of  $0.2 \text{ A g}^{-1}$ , the specific capacity of the LIC full-cell with operating voltage from  $0$  to  $4 \text{ V}$  is  $105 \text{ mA h g}^{-1}$ , corresponding to a specific capacitance of  $94 \text{ F g}^{-1}$ . Based on the mass of the cathode, the specific capacity is  $121 \text{ mA h g}^{-1}$  (specific capacitance:  $108 \text{ F g}^{-1}$ ), indicating nearly 92% utilization of the SG cathode ( $118 \text{ F g}^{-1}$  at a current density of  $0.2 \text{ A g}^{-1}$ ). The rate performance of this dual-graphene LIC full-cell is similar to that of the AC//LTO LIC full-cell reported by Dsoke *et al.*<sup>10</sup> Fig. 5f compares the CV loops between the SG//SG EDLC and the dual-graphene SG//Li-SG LIC. In comparison with the CV loop of the SG//SG EDLC, the enclosed area of the dual-graphene SG//Li-SG LIC is much larger.

This is due to the hybridization of the two electrodes that enabled the LIC cell to be operable at a higher working voltage. These two factors contribute to the further increase in the energy density and power density of the LIC device. The present

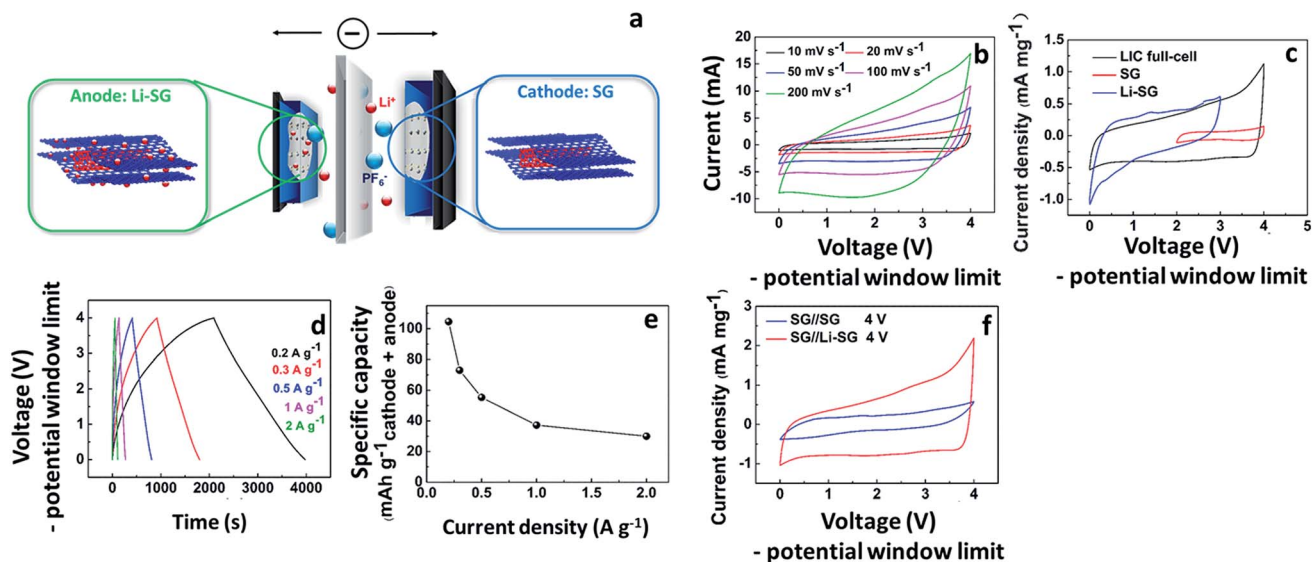


Fig. 5 (a) Schematic illustration of the SG//Li-SG Li-ion capacitor (LIC). (b) Cyclic voltammograms (CV) of the SG//Li-SG LIC device at different scan rates. (c) Comparison of CVs for the SG cathode (2–4 V), Li-SG anode (0.01–3 V), and SG//Li-SG LIC full cell (0.01–4 V) at a scan rate of 10  $\text{mV s}^{-1}$ . (d) Galvanostatic charge–discharge curves at increasing current densities. (e) Rate performance of the SG//Li-SG LIC full cell (0.01–4 V). (f) Comparison of CVs at a scan rate of 20  $\text{mV s}^{-1}$  between the SG//Li-SG LIC cell and SG//SG capacitor in the potential window from 0.01 to 4 V.

dual-graphene SG//Li-SG LIC full-cell delivered a high energy density of  $209 \text{ W h kg}^{-1}$  under operating voltage from 0 to 4 V, which is about five times that of the SG//SG EDLC.

A three-electrode cell (SG//Li//Li-SG) was assembled to investigate the electrochemical behaviour of the SG cathode and the Li-SG anode. In the three-electrode cell, a lithium foil was used as the reference electrode to record the electrochemical signals of the SG cathode and the Li-SG anode. As shown in

Fig. 6a–d, the dark curves indicate that the absorption and desorption of  $\text{PF}_6^-$  ions on the surface of the SG cathode took place above 2 V as designed. The blue curves indicate the intercalation and de-intercalation of  $\text{Li}^+$  ions on the Li-SG anode. It should be noted that, when the operating voltage of the SG//Li//Li-SG cell was 3.5 V (Fig. 6a) and 3.7 V (Fig. 6b), the  $\text{Li}^+$  ions would not have been fully intercalated into the Li-SG electrode since the potential of the Li-SG electrode was at

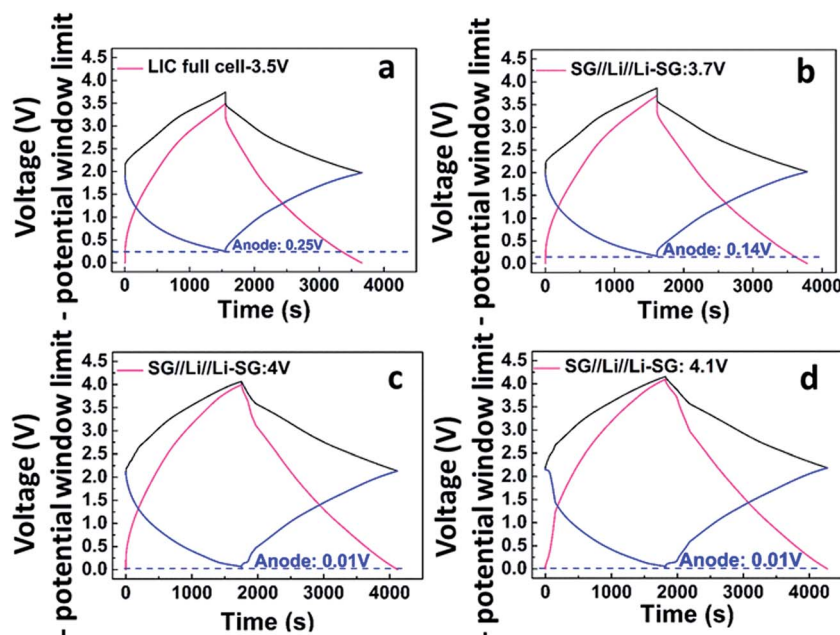


Fig. 6 Cathode, anode, and LIC full-cell potential profiles at a current density of  $0.2 \text{ A g}^{-1}$  with increasing potential windows for the three-electrode SG//Li//Li-SG cell at (a) 3.5 V; (b) 3.7 V; (c) 4.0 V; and (d) 4.1 V.

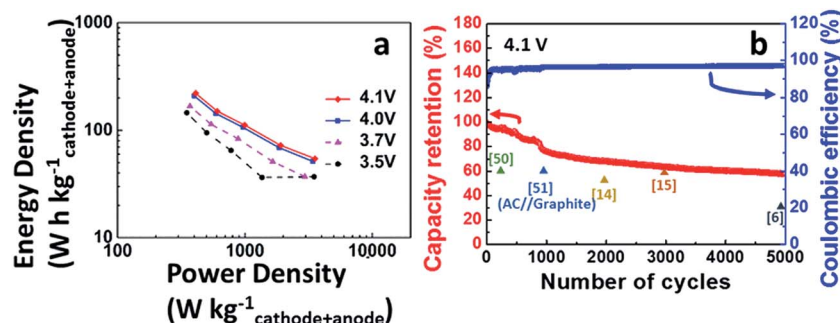


Fig. 7 (a) Ragone plot of the SG//Li-SG LIC full cell operated under various conditions. Highest energy density of  $222 \text{ W h kg}^{-1}$  was obtained with a power density of  $410 \text{ W kg}^{-1}$ . (b) Cycling performance of the SG//Li-SG LIC full cell operated between 0.01 and 4.1 V at a current density of  $0.2 \text{ A g}^{-1}$ .

0.25 and 0.14 V, respectively. As an indicator, the capacity of the hybrid LIC full-cell cannot reach the utmost, leading to lower energy densities as shown by dark and pink lines in Fig. 7a. When the operating voltage of the SG//Li//Li-SG cell was increased to 4.0 V (Fig. 6c) and 4.1 V (Fig. 6d), the potential of the anode was further reduced to 0.01 V, indicating that  $\text{Li}^+$  ions were fully intercalated to saturation into the anode. The full-lithiation of the anode resulted in even higher energy densities as shown by the blue and red lines in Fig. 7a. As depicted in Fig. 7a, the energy density of the dual-graphene LIC reached  $222 \text{ W h kg}^{-1}$  at the power density of  $410 \text{ W kg}^{-1}$  under a working voltage of 4.1 V.

To indicate the energy densities delivered by LIC devices employing different electrode materials, Table 1 summarizes the energy performances of various LIC structures reported to date in the literature. The energy density (ED) achieved in the LIC devices with SG//Li-SG electrodes from this study is comparable to the result obtained with devices using functionalized graphene and reduced graphene oxide electrodes,<sup>14</sup> but is considerably higher than that from similar

devices using other materials as the anode and cathode. Fig. 7a shows the energy density *versus* power density of the LIC devices. The possible over-estimate of the energy density due to the formation of SEI film is estimated to be less than 9% as discussed in Section 2.3. If we consider that the potential window should be the same as that for commercial AC//graphite LICs, the energy density of our SG//Li-SG LICs would decrease to  $158 \text{ W h kg}^{-1}$  and the power density to  $290 \text{ W kg}^{-1}$ . Besides the energy density, the cycling performance of the LIC cells employing SG//Li-SG electrodes demonstrates noticeable improvement. The cycling performance of the SG//Li-SG LIC full-cell operated between 0.01 and 4.1 V at the current density of  $0.2 \text{ A g}^{-1}$  is shown in Fig. 7b. The coulombic efficiency was maintained at 97% after 5000 cycles, indicating that the charge/discharge process is highly reversible in this SG//Li-SG LIC full-cell. The capacity retention dropped from 100% to 75% only after initial 1000 cycles, and to 58% after 5000 cycles. Such a retention in capacity is about twice that of a  $\text{Li}_4\text{Ti}_5\text{O}_{12}$ /poly(methyl)thiophene LIC,<sup>6</sup> and is much higher than that of a typical AC//graphite LIC<sup>51</sup> and those of pure graphene-based LICs,<sup>14</sup> due to the faradaic reactions, the cycling performance of the LIC is sacrificed in order to achieve higher energy density in comparison with the EDLC. Nonetheless, the cycling stability of the graphene LIC is still much greater than that reported for LIBs (50–80% in the 300<sup>th</sup> cycle).<sup>52</sup>

Table 1 The energy density of the lithium-ion capacitor reported<sup>a</sup>

No.	Anode	Cathode	ED ( $\text{W h kg}^{-1}$ )	Ref.
1	$\text{Li}_4\text{Ti}_5\text{O}_{12}$	AC	85	4
2	$\text{MnO}_2/\text{CNT}$	$\text{LiMn}_2\text{O}_4$	56	5
3	$\text{Li}_4\text{Ti}_5\text{O}_{12}$	Poly(methyl)thiophene	56	6
4	Graphite	AC	103.8	7
5	Nickel oxide	AC	$108 (\text{J cm}^{-3})$	8
6	$\text{Mn}_x\text{O}_y$	AC	21	9
7	$\text{Li}_4\text{Ti}_5\text{O}_{12}$	AC	33	10
8	Carbon black	C/LiFePO <sub>4</sub>	7	11
9	Graphene	AC	61.7	12
10	$\text{Li}_4\text{Ti}_5\text{O}_{12}/\text{C}$	Graphene	72	13
11	Reduced graphene oxide	Functionalized graphene	225	14
12	Camera flash reduced GO	Porous 3D graphene-based carbon	148.3	15
13	Li-SG	SG	222	This work

<sup>a</sup> ED: energy density.

## 4. Conclusions

In summary, we have designed, fabricated, and characterized a hybrid lithium-ion capacitor (LIC) using asymmetric graphene electrodes made of a single-wall carbon nanotube and graphene (SG) composite. The pre-lithiated SG anode delivered a maximum reversible capacity of  $500 \text{ mA h g}^{-1}$ . Its capacity represents a significant improvement over that of a graphite anode (theoretical maximum capacity of a graphite anode is  $372 \text{ mA h g}^{-1}$ ). The energy density of the SG//Li-SG LIC reached  $222 \text{ W h kg}^{-1}$ . These results suggest that hybrid LICs with asymmetric SG electrodes offer a promising opportunity for developing energy storage devices with a good cycling stability and high energy density while retaining a high power density.

## Acknowledgements

This work was supported by the NIMS microstructural characterization platform as a program of “Nanotechnology Platform” of the Ministry of Education, Culture, Sports, Science and Technology (MEXT), Japan. This study was also supported by the Shandong Taishan Scholar Program and a fellowship from the Japan Society for the Promotion of Science (JSPS).

## References

- 1 F. Béguin and E. Frąckowiak, *Supercapacitors: Materials, Systems, and Applications*, Wiley-VCH Verlag GmbH & Co., Weinheim, 2013.
- 2 B. E. Conway, *J. Electrochem. Soc.*, 1991, **138**, 1539.
- 3 J. R. Dahn and J. A. Seel, *J. Electrochem. Soc.*, 2000, **147**, 899.
- 4 G. G. Amatucci, F. Badway, A. D. Pasquier and T. Zheng, *J. Electrochem. Soc.*, 2001, **148**, A930.
- 5 S.-B. Ma, K.-W. Nam, W.-S. Yoon, X.-Q. Yang, K.-Y. Ahn, K.-H. Oh and K.-B. Kim, *Electrochem. Commun.*, 2007, **9**, 2807.
- 6 A. D. Pasquier, A. Laforgue and P. Simon, *J. Power Sources*, 2004, **125**, 95.
- 7 V. Khomenko, E. Raymundo-Piñero and F. Béguin, *J. Power Sources*, 2008, **177**, 643.
- 8 M.-S. Park, Y.-G. Lim, J.-H. Kim, Y.-J. Kim, J. Cho and J.-S. Kim, *Adv. Energy Mater.*, 2011, **1**, 1002.
- 9 V. Khomenko, E. Raymundo-Piñero and F. Béguin, *J. Power Sources*, 2006, **153**, 183.
- 10 S. Dsoke, B. Fuchs, E. Gucciardi and M. W. Mehrens, *J. Power Sources*, 2015, **282**, 385.
- 11 A. Krause, P. Kossyrev, M. Oljaca, S. Passerini, M. Winter and A. Balducci, *J. Power Sources*, 2011, **196**, 8836.
- 12 J. J. Ren, L. W. Su, X. Qin, M. Yang, J. P. Wei, Z. Zhou and P. W. Shen, *J. Power Sources*, 2014, **264**, 108.
- 13 S. Li and X. Wang, *J. Power Sources*, 2015, **282**, 394.
- 14 H. Kim, K. Y. Park, J. Hong and K. Kang, *Sci. Rep.*, 2015, **4**, 5278.
- 15 T. Zhang, F. Zhang, L. Zhang, Y. Lu, Y. Zhang, X. Yang, Y. Ma and Y. Huang, *Carbon*, 2015, **92**, 106.
- 16 A. K. Geim and K. S. Novoselov, *Nat. Mater.*, 2007, **6**, 183.
- 17 T. Lin, I. W. Chen, F. Liu, C. Yang, H. Bi, F. Xu and F. Huang, *Science*, 2015, **350**, 1508.
- 18 M. D. Stoller, S. Park, Y. Zhu, J. An and R. S. Ruoff, *Nano Lett.*, 2008, **8**, 3498.
- 19 F. Zhang, J. Tang, N. Shinya and L.-C. Qin, *Chem. Phys. Lett.*, 2013, **584**, 124.
- 20 K. Naoi, S. Ishimoto, J. I. Miyamoto and W. Naoi, *Environ. Sci.*, 2012, **5**, 9363.
- 21 Z. S. Wu, W. Ren, L. Xu, F. Li and H.-M. Cheng, *ACS Nano*, 2011, **7**, 5463.
- 22 J. Wu, X. Qin, H. Zhang, Y.-B. He, B. Li, L. Ke, W. Lv, H. Du, Q.-H. Yang and F. Kang, *Carbon*, 2015, **84**, 434.
- 23 Q. Cheng, J. Tang, J. Ma, H. Zhang, N. Shinya and L.-C. Qin, *Phys. Chem. Chem. Phys.*, 2011, **13**, 17615.
- 24 M. W. Forney, M. J. Ganter, J. W. Staub, R. D. Ridgley and B. J. Landi, *Nano Lett.*, 2013, **13**, 4158.
- 25 G. Gourdin, P. H. Smith, T. Jiang, T. N. Tran and D. J. Qu, *J. Electroanal. Chem.*, 2013, **688**, 103.
- 26 Z. Yang, M. C. Dixon, R. A. Erck and L. Trahey, *ACS Appl. Mater. Interfaces*, 2015, **7**, 26585.
- 27 D. R. Dreyer, S. Park, C. W. Bielawski and R. S. Ruoff, *Chem. Soc. Rev.*, 2010, **39**, 228.
- 28 A. C. Ferrari and D. M. Basko, *Nat. Nanotechnol.*, 2013, **8**, 235.
- 29 B. You, L. Wang, L. Yao and J. Yang, *Chem. Commun.*, 2013, **49**, 5016.
- 30 A. Jorio, E. H. M. Ferreira, M. V. O. Moutinho, F. Stavale, C. A. Achete and R. B. Capaz, *Phys. Status Solidi B*, 2010, **247**, 2980.
- 31 A. C. Ferrari, S. E. Rodil and J. Robertson, *Phys. Rev. B: Condens. Matter Mater. Phys.*, 2003, **67**, 155306.
- 32 L. Zhang, F. Zhang, X. Yang, G. Long, Y. Wu, T. Zhang, K. Leng, Y. Huang, Y. Ma, A. Yu and Y. Chen, *Sci. Rep.*, 2013, **3**, 1408.
- 33 S. Zhang and N. Pan, *Adv. Energy Mater.*, 2014, **5**, 1401401.
- 34 Y. Zhu, S. Murali, M. D. Stoller, K. J. Ganesh, W. Cai, P. J. Ferreria, A. Pirkle, R. M. Wallace, K. A. Cychoz, M. Thommes, D. Su, E. A. Stach and R. S. Ruoff, *Science*, 2011, **332**, 1537.
- 35 Q. Cheng, J. Tang, N. Shinya and L.-C. Qin, *J. Power Sources*, 2013, **241**, 423.
- 36 W. Yuan, Y. Zhang, L. Cheng, H. Wu, L. Zheng and D. Zhao, *J. Mater. Chem. A*, 2016, **4**, 8932.
- 37 S. Paulson, A. Helser, N. M. B. Nardelli, R. M. Taylor, M. Falvo, R. Superfine and S. Washburn, *Science*, 2000, **290**, 1742.
- 38 B. Baowan, J. B. Cox and J. M. Hill, *Carbon*, 2007, **45**, 2972.
- 39 D. Yu and L. Dai, *J. Phys. Chem. Lett.*, 2010, **1**, 467.
- 40 D. Jena, T. Fang and Q. Zhang, *Appl. Phys. Lett.*, 2008, **93**, 112.
- 41 M. Kim, F. Xu, J. H. Lee, C. Jung, S. M. Hong, Q. M. Zhang and C. M. Koo, *J. Mater. Chem. A*, 2014, **2**, 10029.
- 42 L. Zeng, C. Zheng, L. Xia, Y. Wang and M. Wei, *J. Mater. Chem. A*, 2013, **1**, 4293.
- 43 L. Zeng, F. Xiao, J. Wang, S. Gao, X. Ding and M. Wei, *J. Mater. Chem.*, 2012, **22**, 14284.
- 44 R. Yazami and M. Deschamps, *J. Power Sources*, 1995, **54**, 411.
- 45 J. S. Xue and J. R. Dahn, *J. Electrochem. Soc.*, 1995, **142**, 3668.
- 46 S. Wang, Y. Matsumura and T. Maeda, *Synth. Met.*, 1995, **71**, 1759.
- 47 K. Sato, M. Noguchi, A. Demachi, N. Oki and M. Endo, *Science*, 1994, **264**, 556.
- 48 J. Li and F. Gao, *J. Power Sources*, 2009, **194**, 1184.
- 49 J. P. Zheng, *J. Electrochem. Soc.*, 2003, **150**, A484.
- 50 S. R. Sivakkumar, A. S. Milev and A. G. Pandolfo, *Electrochim. Acta*, 2011, **56**, 9700.
- 51 H. Wang and M. Yoshio, *J. Power Sources*, 2008, **177**, 681.
- 52 X. Li, J. Liang, Z. Hou, W. Zhang, Y. Wang, Y. Zhu and Y. Qian, *J. Power Sources*, 2015, **293**, 868.